Experimental Investigation and Modeling of Copper Smelting Slags

KONSTANTIN STARODUB, YAROSLAVA KUMINOVA, ALAN DINSDALE, VLADIMIR CHEVERIKIN, VERA FILICHKINA, ABDUKAHHAR SAYNAZAROV, ALEXANDRA KHVAN, and ALEX KONDRATIEV

Effective extraction of copper from sulfide ores requires careful operation of a copper smelter, which in turn depends very much on chemistry of the feed and resulted slag and matte. For example, chemical composition of copper smelting slags has to be in a certain range to ensure that their properties are within specific limits. Disobeying these rules may lead to complications in smelting operation, poor quality of the copper products, and premature shutdown of the copper smelter. In the present paper the microstructure and phase composition of slags from the Almalyk copper flash smelter were investigated experimentally and then modeled thermodynamically to evaluate potential ways of improvement and optimization of the copper smelting process and its products. The slag samples were taken at different stages of the copper smelting process: on slag tapping, after slag transportation to a deposition site, and at the site. Experimental investigation included the XRD, XRF, and SEM techniques, which were also confirmed by the traditional wet chemistry analysis. Thermodynamic modeling was carried out using thermochemical software package MTDATA, which enables thermodynamic and physical properties of the matte, slag, and gas phases to be calculated in a wide range of temperatures, pressures, and chemical compositions. In addition, slag viscosities and corresponding matte settling rates were estimated using the modified Urbain and Utigard–Warczok models, and the Hadamard–Rybczynski equation, respectively. It was found that the copper content in the slags may vary significantly depending on the location of slag sampling. Cu was found to be present as sulfide particles, almost no Cu was found to be dissolved in the slag. Analysis of microstructure and phase composition showed that major phase found in the samples is fayalite, while other phases are complex spinels (based on magnetite), different sulfides, and a glass-like phase. Thermodynamic calculations demonstrated the presence of these phases, their compositions, and optimal ranges of operating conditions. Potential ways of improving the matte grade and optimizing the smelting process were suggested on the basis of the calculations.

DOI: 10.1007/s11663-016-0761-3

I. INTRODUCTION

A number of metallurgical plants utilize a flash smelting process (Outotec or Inco) in the extraction of copper from sulfide ores. In this continuous process fine particles of the Cu-Fe-S concentrate, SiO_2 flux, and O_2 (or air) are fed into a hot 1473 K to 1573 K (1200 °C to 1300 °C) smelting furnace, where the sulfide particles react rapidly with oxygen, thereby converting sulfur into SO_2 gas and producing molten matte and slag.

The matte phase consists mostly of Cu-Fe sulfides, while the major components of the slag phase are FeO, Fe_2O_3, and SiO_2, with small additions of other oxides like Al_2O_3, CaO, *etc*. Furthermore, the percentage of ferrous oxide in slag is much greater than that of ferric oxide, because the oxygen potential in the slag is normally very low. The copper smelting slags are usually referred to as the fayalite slags, since fayalite (Fe_2SiO_4) is one of the main phases crystallized on cooling. However, as found in the present paper, even at a particular smelter the slag composition can change significantly during its operation depending on the feed quality and composition and on smelting conditions.

The essential goal of a matte smelting process (such as flash smelting) is to recover as much Cu from the concentrate into the molten matte as possible. The matte grades (the Cu percentage) can vary depending on the Cu content in the original ore and on the type and

KONSTANTIN STARODUB, Ph.D. Student, ALAN DINSDALE, Lead Research Fellow, VLADIMIR CHEVERIKIN and ALEX KONDRATIEV, Senior Research Fellows, and ALEXANDRA KHVAN, Director, are with the SRC Thermochemistry of Materials, National University of Science and Technology MISIS, Leninskiy Prospect, 4, Moscow, Russia 119049. Contact e-mail: starodub@misis.ru YAROSLAVA KUMINOVA, Ph.D. Student, and VERA FILICHKINA, Head of the Department, are with the Department of Standardization and Quality Control, National University of Science and Technology MISIS. ABDUKAHHAR SAYNAZAROV, Chief Metallurgist, is with the JSC Almalyk GMK, Amir Temur St., 53, Almalyk, Tashkent Region, Republic of Uzbekistan.

Manuscript submitted December 25, 2015.
Article published online July 27, 2016.

operating conditions of the smelting furnace. Poor extraction of copper from the concentrate leads to significant copper losses with slag wastes (*e.g.*, Reference 1). To reduce copper losses a detailed understanding of the matte-slag chemistry is necessary.

In the present work a number of slag samples taken from different stages of an Inco flash smelting process located at Almalyk (Republic Uzbekistan) were investigated experimentally by conventional microstructure and analytical techniques and theoretically by the computational thermodynamics method to achieve better understanding of the process and to evaluate possible ways of process improvement and reduction of copper losses.

Ten slag samples were taken from different steps of the Almalyk flash smelting process: at a slag deposition site, during slag tapping, and from the crust formed at the bottom of a slag ladle while being transported to a deposition site. These slag samples were analyzed by the X-ray diffraction (XRD), light and scanning electron microscopy (LM and SEM), X-ray fluorescence (XRF), and wet chemistry methods and were modeled using the thermodynamic software MTDATA.[2] In the present paper the results of the experimental study and modeling are presented and discussed.

II. EXPERIMENTAL

A. *X-ray Diffraction*

The XRD analysis was carried out on a D8 Discover X-ray diffractometer (Bruker-AXS, Germany). The X-ray 1.6kWt tube with a copper anode was taken as an X-ray source. Parallel beam with a divergence 0.03 deg was formed by a Goebel mirror. The width of an X-ray beam was 0.2 mm. Reflected beam intensity was measured with a position-sensitive detector LynxEye (angular resolution 0.015 deg). In front of the detector Ni filter was installed. In order to reduce the X-ray fluorescence influence (samples contain significant amounts of iron) detector's discriminator window was narrowed, thus improving the signal-to-noise ratio. Measurements were carried out by the 2θ–ω scheme.

Average measurement time to obtain one diffraction pattern is 6 to 7 hours. The background from a quartz glass substrate (sample holder) was first subtracted from the diffraction pattern. Then the phase analysis was performed with the EVA software and database ICDD PDF-2 2004.[3]

B. *X-ray Fluorescence and Wet Chemistry Analysis*

The X-ray fluorescence analysis was carried out with a X50 Mobile spectrometer in order to measure the amount of copper in each sample. At first small amounts (around 15 g) of each sample were grinded in a ring vibratory Herzog H100 using a tungsten carbide mortar. The analysis was carried out simultaneously with three X-rays: a 50 kV tube (for heavy elements), 35 kV (for transit metals), and 15 kV (for light elements). Instrument provides results between 0 to 1 pct—up to 4 decimal places, in excess of one percent—up to two. For each sample three parallel measurements were carried out.

The Cu content in the slag samples was also verified by a traditional wet chemistry analysis that was based on titration of iodine by the sodium thiosulfate solution. This method is also called the iodometric titration or iodometry and can be used for a precise determination of the Cu amount in a range of 0.05 to 60 wt pct.

C. *Light and Scanning Electron Microscopy*

Light microscopy was employed to obtain a general view of the sample structure, porosity, and approximate sulfide particle size and distribution using a metallographic Olympus GX71F-5 microscope with the magnification from 12.5 to 1000 times.

Microstructure investigation was carried out with an electron scanning microscope TESCAN VEGA LMH (with LaB_6 cathode) equipped with an X-ray EDS microanalysis system "Advanced AZtecEnergy" by Oxford Instruments. Prior to the SEM EDS analysis, the slag samples were mold into an epoxy resin, polished, and covered with carbon film to provide electrical conductivity.

D. *Thermodynamic Calculations*

Chemical equilibrium in the "matte-slag-gas" system was calculated with the elemental chemical compositions obtained by the SEM EDS analysis using the MTDATA software[2] and NPLOX database (National Physical Laboratory, UK). The oxygen content was balanced on the basis of the assumption that all the elements except sulfur are present in the slag phase as most stable oxides.

III. RESULTS AND DISCUSSION

A. *Chemical Analysis of the Slag Samples*

The average chemical composition of the slag samples was determined by the SEM element mapping and is shown in Table I (the oxygen content is balanced to 100 at pct). The mapping area was a square typically with a side of 0.5 to 1 mm, so the investigated area of a sample was about 0.3 to 1 mm^2. All elements of the periodic table heavier than Li were identified in the mapping spectra. Samples ##1–8 were taken from the slag deposition site, samples #9 (A, B, and D) were from the ladle bottom crust (from different zones), and sample 10 was taken on slag tapping.

The normalized slag chemical compositions plotted on the MeO-FeO-SiO_2 pseudoternary diagram, where MeO is a sum of all other oxides (Al_2O_3, CaO, MgO, *etc*), are shown in Figure 1. It was assumed for simplicity that the Fe_2O_3 content in the slag phase is negligible, so all iron can be represented as ferric oxide. The ratio of FeO/SiO_2 corresponding to the fayalite composition is showed as a dotted blue line. It can be seen from this figure that only three slag samples (##4, 6, and 9) could be considered as a true fayalite slag (*i.e.*,

Table I. The Elemental Chemical Composition of the Slag Samples, Atomic Percent (O is Balanced)

##	Mg	Al	Si	S	K	Ca	Ti	Cr	Mn	Fe	Cu	Zn	Ba	Pb
1	1.45	4.20	15.21	2.10	1.11	1.60	0.12	0.02	0.17	18.54	0.38	0.44	0.05	0.03
2	0.78	4.21	20.75	0.47	1.32	1.17	0.14	0.07	12.20	12.20	0.74	0.36	0.05	0.11
3	0.00	4.69	17.00	0.63	1.10	1.32	0.15	0.00	0.13	16.00	0.21	0.87	0.00	0.08
4	0.00	2.52	12.30	1.11	1.21	0.89	0.05	0.00	0.00	26.25	0.71	0.23	0.00	0.03
5	0.00	4.84	18.98	1.04	1.33	1.37	0.25	0.00	0.03	14.48	0.22	0.36	0.00	0.03
6	0.00	2.18	6.09	11.70	0.36	0.28	0.06	0.00	0.00	29.60	6.23	0.57	0.00	0.18
7	0.46	2.66	30.2	0.70	1.53	0.59	0.07	0.01	0.02	4.09	0.14	0.07	0.02	0.04
8	0.92	4.12	19.21	0.50	1.57	1.00	0.21	0.10	0.06	15.40	0.26	0.38	0.04	0.04
9A	0.68	4.43	30.04	0.4	1.68	1.06	0.18	0.00	0.05	14.07	0.25	0.21	0.00	0.00
9B	0.00	2.7	20.8	0.7	1.0	0.5	0.1	0.00	0.1	22.5	1.2	0.3	0.00	0.1
9D	0.00	4.1	27.1	0.9	1.3	2.0	0.2	0.00	0.1	11.3	0.3	0.2	0.00	0.00
10	0.80	3.10	25.4	0.30	1.30	0.70	0.20	0.00	0.00	14.50	0.50	0.30	0.00	0.10

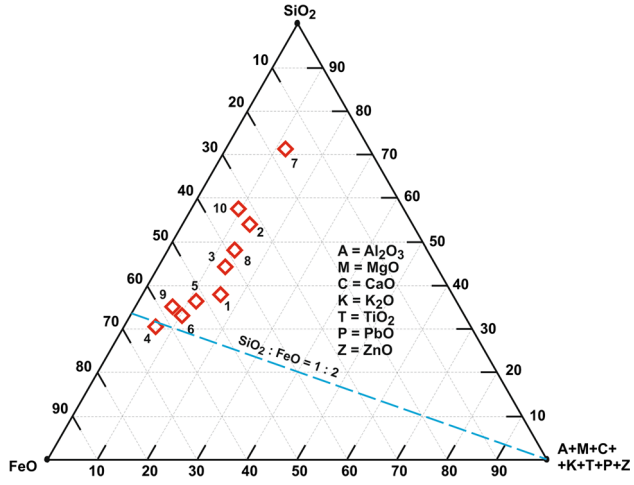

Fig. 1—Pseudoternary diagram of the MeO-FeO-SiO_2 (mol pct).

with the SiO_2/FeO ratio around 1/2). Samples #1 and #5 are close enough to the demanded ratio, but samples ##2, 7, and 10 contain SiO_2 greater than 50 molar pct. Samples #3 and #8 lay in between. Sample #7 was found to contain undissolved quartz ore particles used as a flux in the flash smelting process.

It should also be noted that the SEM EDS analysis cannot determine the oxidation state of iron in the slag, and other methods should be used to distinct between ferrous and ferric iron. In the present work, whether it was possible, phase determination by SEM EDS was corrected according to the XRD results.

The amount of copper determined by the SEM EDS element mapping, XRF, and wet chemistry methods are shown in the Figure 2. It can be seen that the Cu amount in the slag samples from the deposition site varies significantly, from 0.45 up to 7.98 wt pct. Compared to the amount of copper in the sample from tapping, there are five samples with a lower percentage of Cu and three with a higher percentage. The average amount of copper in these samples measured by the wet chemistry method is 1.9 wt pct. It should be mentioned that the ladle bottom sample (#9) consists of three different zones, and the Cu content of each zone was measured separately by SEM, XRF, and wet chemistry.

It can also be seen from Figure 2 that the local SEM EDS method provides values of the Cu amount comparable with those by the XRF and titrimetry methods for most of the samples.

The preceding sections provide results of the microstructure analysis that are divided into three groups, depending on the sampling location: on slag tapping (sample #10), at the deposition site (samples ##1–8), and from the ladle bottom (sample #9).

B. *Slag Sample from Tapping*

Slag samples taken on slag tapping are usually quenched into water right after they have been collected; therefore, these samples are likely to be the closest to the original state, in which the molten slag phase is inside the smelting furnace. Figure 3 represents a typical picture of the slag sample #10 taken during slag tapping and quenched thereafter.

Figure 4 shows a LOM image of slag #10. It can be seen that most of the sulfide particles are very fine (<1 μm) and formed apparently during rapid cooling. The average size of the fine sulfides was estimated to be less than 200 to 300 nm. Bigger particles (≥1 to 2 μm) are likely to be entrapped from matte due to a number of factors (for example, higher slag viscosity).

Despite a lot of noise, the XRD pattern (Figure 5) showed strong, distinctive peaks (marked blue) that can clearly be identified as the fayalite (Fe_2SiO_4) phase. Other peaks are less distinctive, rather broad and small, and cannot conclusively be analyzed. Some of these peaks (marked red) may be attributed to a magnetite-like phase (*e.g.*, Fe_3O_4) with other atoms (*e.g.*, Al, Mg, *etc*) introduced into the structure. Formation of the magnetite phase is typical for copper smelting slags (*e.g.*, References 4 and 5).

The SEM EDS analysis revealed at least two different regions in the slag (Figure 6(a)): a region with the average 1Fe:2Si stoichiometry (balanced with oxygen) and a copper sulfide phase with the approximate Cu_2S stoichiometry. The former oxide "phase" appears to be a mixture of two finely dispersed regions slightly different by the backscattered electron contrast (one is brighter, other is darker), as the EDS spectra of each of these regions differ by 1 to 2 at pct of Fe from each

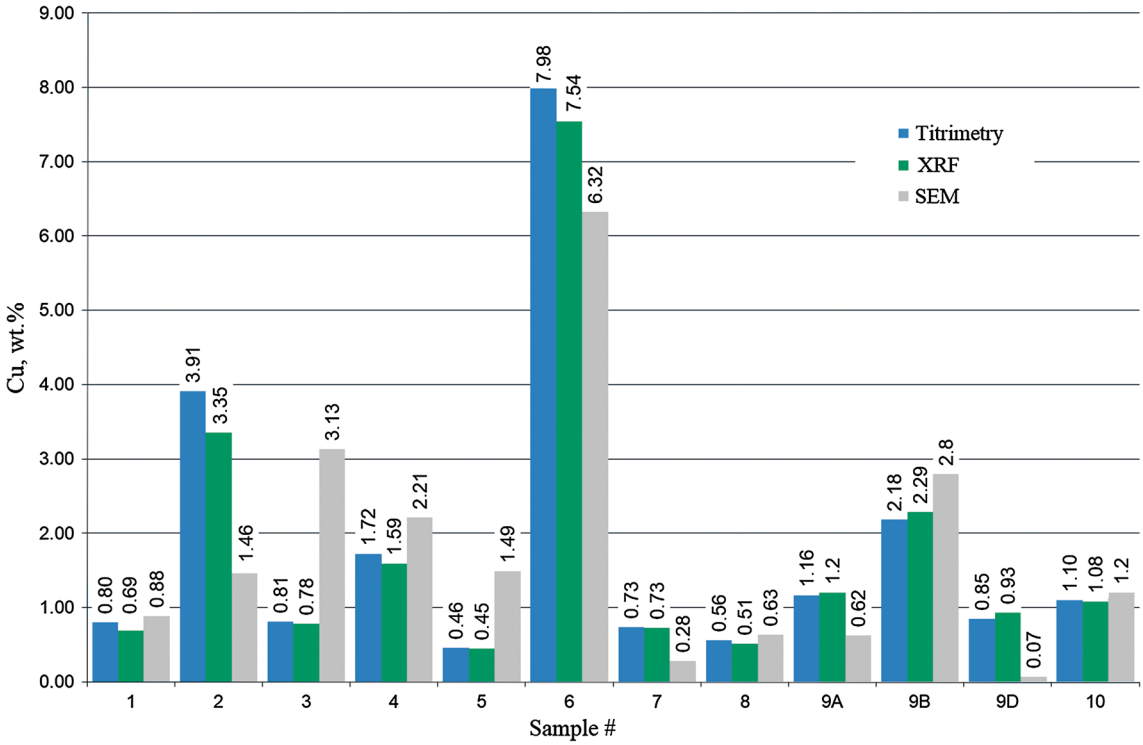

Fig. 2—The amount of Cu (wt pct) in the slag samples obtained by different methods.

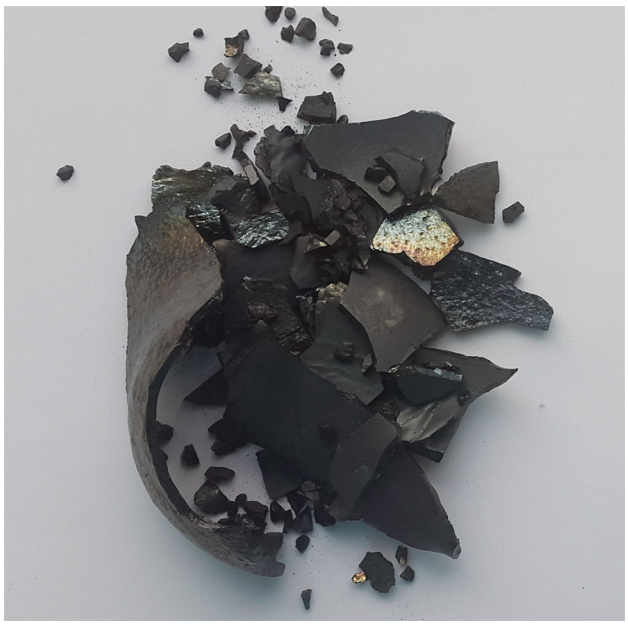

Fig. 3—The slag sample #10 taken during slag tapping.

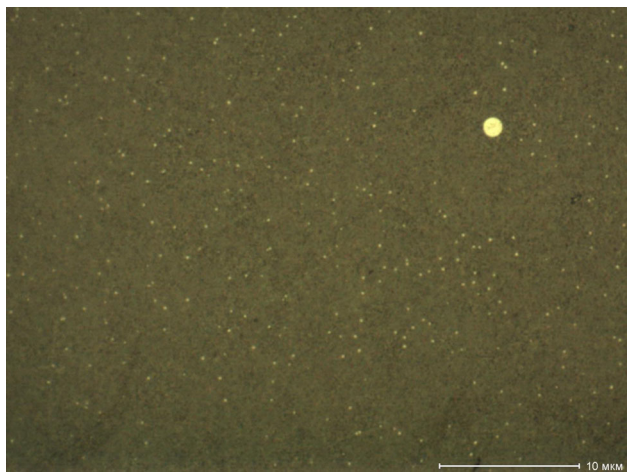

Fig. 4—A LOM image of the slag sample #10.

other. It contains small amounts of Al, Ca, Mg, K, and Ti as well as up to 1 wt pct Cu and ~0.3 to 0.5 wt pct of S. The copper sulfide phase can contain a moderate amount of Fe (up to 5 to 10 at pct) and consists of scattered spherical particles with the diameter varying from 0.1 to 200 μm. Since a $FeSi_2O_5$-like phase is not known, it can be assumed based on the XRD results that the fayalite crystals are very small and scattered in a matrix (a glassy phase) and cannot be detected with the SEM EDS analyser. The other phase found by SEM is magnetite (Figure 6(b)) surrounded by a glassy phase with fayalite crystals.

The amount of copper in the sample determined by X-ray fluorescence is 1.03 wt pct (±0.01 wt pct), while the amount of copper determined by titration is 1.0995 wt pct (±0.01 wt pct). The experimental error for this sample and other samples was calculated from the mean root squares for a series of measurements for each sample.

Figures 6(a) and 7 depict the SEM EDS image and element mapping of an area about 0.4 mm^2 for the slag

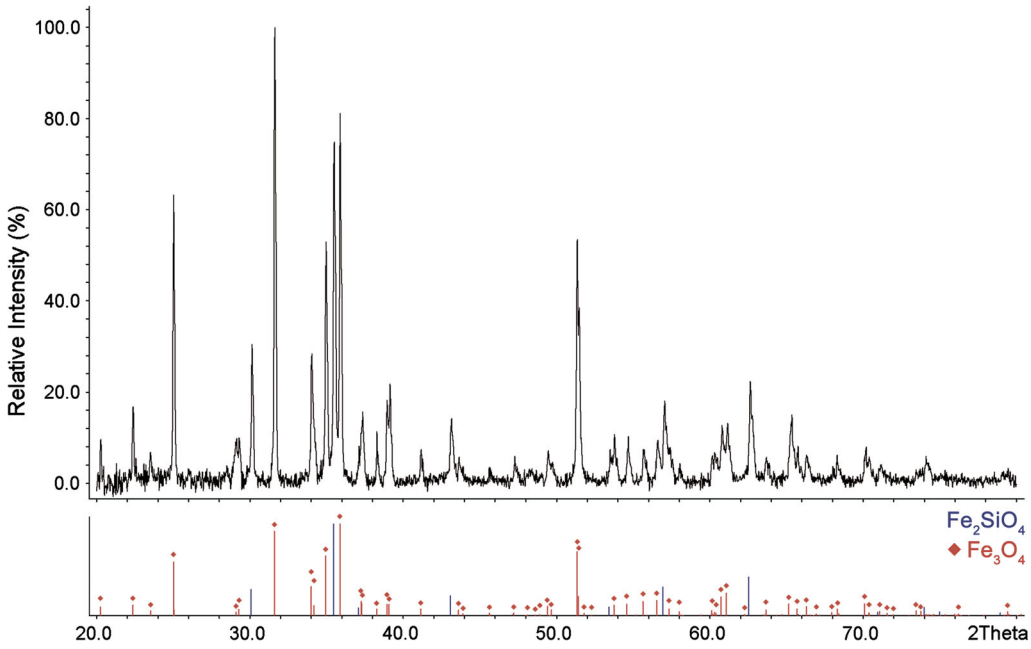

Fig. 5—XRD graph for the slag sample #10.

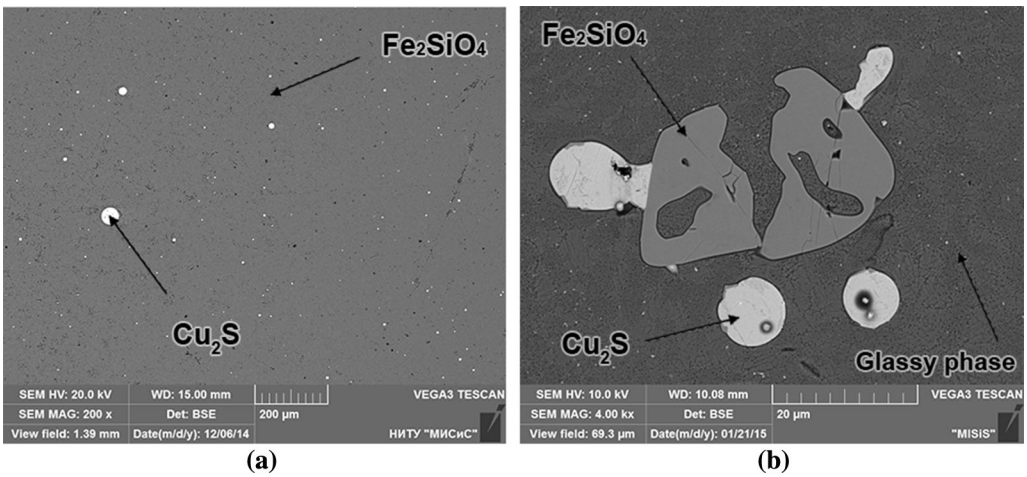

Fig. 6—(*a*) A typical microstructure and (*b*) magnetite particles found in sample #10.

sample #10. It could be seen that the sample looks fairly uniform, which may indicate that crystals are very fine or the sample is in the amorphous state.

C. *Slag Samples from the Deposition Site*

Eight slag samples were taken from the slag deposition site. The samples were picked up at random from the surface of the recent slag deposit over the area of several square meters. Figure 8 represents a typical picture of these samples. All the samples are remarkably porous (see also Figure 9), have different color of the surface depending on the average composition (red for iron oxide, blue spots for copper oxide, *etc*.)

A LOM image of sample #3 is shown in Figure 9 as an example of typical slag microstructure. Big and small irregular pores as well as bright sulfide particles can be observed in the sample.

A typical XRD pattern for the deposition slag (sample #5) is shown in Figure 10. It reveals mainly the fayalite (blue) and magnetite (red) phases. It can be seen from Figure 10 that other phases are also like to be present, but their exact composition cannot be detected because peaks are very small and indistinctive. The sulfide phases like chalcopyrite, bornite, *etc*. were found likely to be present in these samples.

Summary of the phases found in the slag samples using the SEM EDS and XRD analyses is given in Table II. Most of them include fayalite, copper, and iron sulfides and magnetite. Abbreviations in brackets shown in the "Cu-Fe sulphides" column mean: P—pyrrhotite($Fe_{(1-x)}S$), C—chalcocite (Cu_2S),

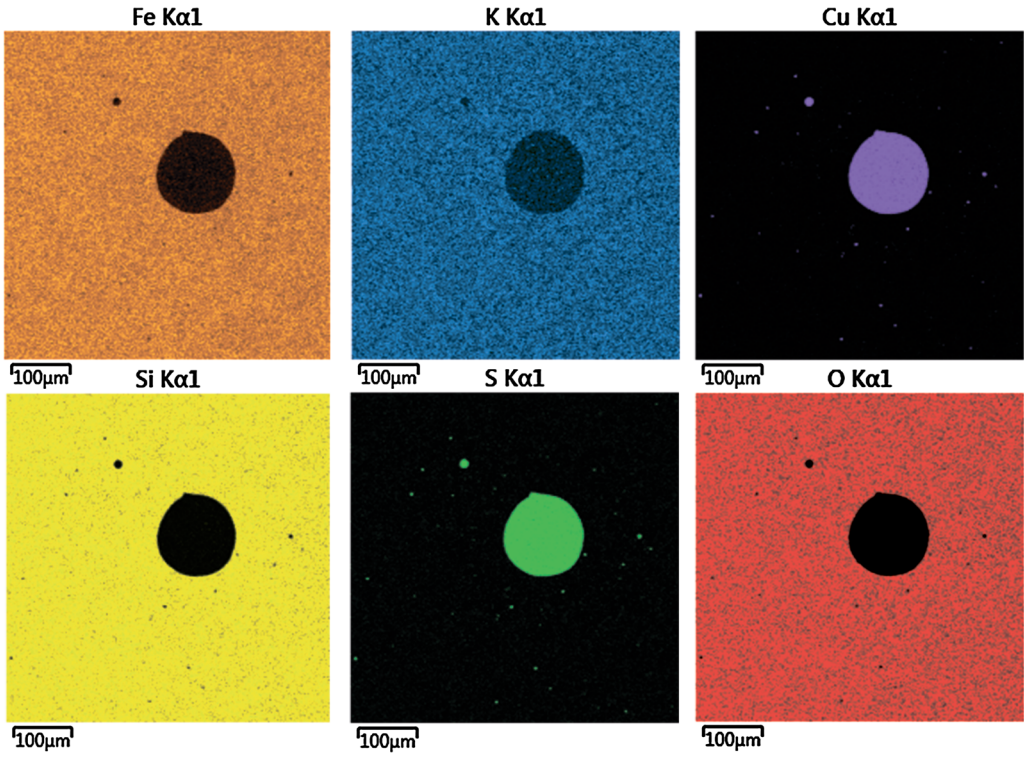

Fig. 7—Element distribution in sample #10.

Fig. 8—Some of the slag samples taken from the deposition site.

R—roxbyite (Cu_9S_5), B—bornite (Cu_5FeS_4), M—marcasite (FeS_2), N—nukundamite ($Cu_{3.4}Fe_{0.6}S_4$). The "Glass" column represents a glassy phase found only by the SEM EDS. The column "Other phases" represents other oxide and/or sulfide phases found in the samples.

An example of evaluation of the phase composition using the SEM EDS phase mapping is given in Figures 11(a) and (b). Different phases are marked by different colors, and their average spectra determined by SEM EDS are listed in Table III. The amount of fayalite (denoted in Table II as "FeOSi") is found to be 75.2 pct of the picture area. The fayalite phase can also contain Ca, Mg, Zn, *etc*. A phase called "glass" (denoted as "FeSiO") was observed in between big fayalite crystals (dark areas in Figure 11(b)). Its composition is rich in SiO_2, and it contains substantial amounts of other elements (Fe, K, Al, Ca). Since this phase was not detected in the XRD spectrum, despite its significant amount (12.4 pct of the sample area), it was assumed to be a glassy phase. The next phase called "Complex Sulphides" represents different sulfides observed in the sample. It can be seen that determination of the magnetite phase (denoted as "FeO") is most difficult

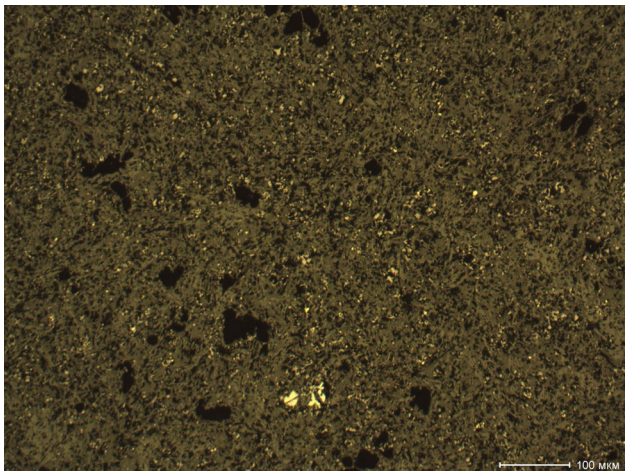

Fig. 9—Typical slag structure (sample #3).

(it can be seen only in Figure 11(a) as bright scattered crystals of irregular shape), but sulfide phases are clearly visible in both Figures 11(a) and (b). The "Magnetite" phase contains Si and Cu, which is due to overlapping of magnetite areas and adjacent areas occupied by the fayalite and other phases. In reality, the magnetite phase in slags was found to contain Al, Ti, and Cr.

Elemental mapping done for the same sample area is given in Figure 12. The magnetite phase can be evaluated by comparison the Si and Fe maps. On the Si map the magnetite crystals are dark, while on the Fe map these areas are brighter than the rest of the map. It can be seen that the percentage of the magnetite phase is much greater than that determined by the phase mapping (Table III). As a result, the fayalite percentage should be less than determined in Table III.

Figure 13 represents typical microstructure found in the sample #7. This sample contains significant amount of SiO_2, most likely undissolved flux particles, which can be seen in Figure 13. Phases marked as A and B are complex silicate phases with the following approximate compositions (determined by SEM EDS): $Si_{23}Fe_{13}Al_4Ca_2MgKO_{69}$ and $Si_{25}Fe_7K_2Al_4MgCaO_{68}$, respectively.

Behavior of minor elements such as Pb, Zn, Ti, *etc*. in the slag samples was also analyzed using the SEM EDS analysis. Pb was found only in a sulfide phase (*e.g*., Figure 14) contrast to Reference 4, where it was reported that around 20 pct Pb should go into the slag phase, while Zn was found to be present mainly in the fayalite and also in sulfide phases (Figure 14). The distribution of Pb and Zn was confirmed by thermodynamic calculations.

Ti and Cr was found to be present only in the magnetite phase, a spinel-type phase; this was also confirmed by thermodynamic calculations. In a number of samples Mo was found to be associated with a sulfide phase, while As, Ba, Mn were found to be present in the slag phases (*e.g*., fayalite, glassy phase, *etc*).

D. *Slag Sample from the Bottom of a Slag Ladle*

The slag sample #9 was taken from the crust formed at the slag ladle bottom. This so-called bottom crust is formed during slag pouring into the ladle and further transportation of the ladle to the slag deposition site by train.

Four zones can be distinguished on the cross section (Figure 15) from the bottom to the top: zone "D" is adjacent to the ladle steel wall and bottom; two zones marked "B", nearly identical in chemical composition and microstructure, are highly porous, found to be rich in sulfides and separated by the interface "C"; zone "A" is a part of the bulk slag. Each zone was investigated separately to obtain information on its microstructure, phase composition, and amount of copper.

The zone A of the sample #9 is a top area in the cross section, the most distant from the ladle bottom. Typical microstructure of this zone is given in Figure 16. Between dendrites of fayalite the SiO_2-rich slag (with SiO_2 ~ 80 mol pct) can be observed. The magnetite phase with dissolved Al and Ti marked as "FeO" in Figure 16 can typically be seen in this zone as big crystals of fairly geometrical shape.

The amounts of copper in the zone A detected by the XRF and titrimetry methods are 1.2 (±0.02) and 1.16 (±0.01) wt pct, respectively.

The interface between zones A and B is shown in Figure 17. It can be seen that the interface is very thin (few μm) and also was found to be very brittle.

Figure 18 illustrates variation of Fe, Cu, Si, Al, and S across the zones A and B scanned along the line marked on the micrograph. The zone A is richer in the Si and Al content, but depleted in the Fe content. It can also be seen that there is a subzone within the zone B with higher amount of copper and sulfur (a Cu-S particle). The elemental mapping for Cu, Fe, K, S, and Si is shown in Figure 19. This figure clearly demonstrates that in the zone B (the right-hand side of the pictures) the amount of S, Cu, and Fe is greater than in the zone A (left-hand side). It can be seen from Figure 19 that Cu is present in the slag as scattered sulfide particles.

The zone B is formed in the middle of the bottom crust. This zone is more porous than the A and D zones and have a different color from the others. As it can be seen in Figures 17, 18, and 19 the zone is not uniform in the vicinity of the interface. A typical microstructure of this zone far from the interface is given in Figure 20.

The average amount of copper in this zone was found to be 2.29 (±0.04) and 2.18 (±0.03) wt pct by XRF and titration, respectively.

Figure 21 represents the zone C, which is an interface zone in the middle of two B zones. Phase composition from both sides of the interface is similar, but the size of crystals is significantly smaller. The interface itself consists mostly of iron oxide, most probably Fe_2O_3, with inclusions of sulfides. It is not quite clear how this interface line was indeed formed; perhaps the reason lies in the exact procedure and timing of pouring liquid slag in the ladle. Small part of molten slag could have been poured into the ladle, crystallized being in contact with oxygen from atmosphere, and then the rest of the slag was poured. This could explain oxide film layer and smaller grain size. The width of the iron oxide interface is significantly larger than that for the A–B interface and is about 20 μm.

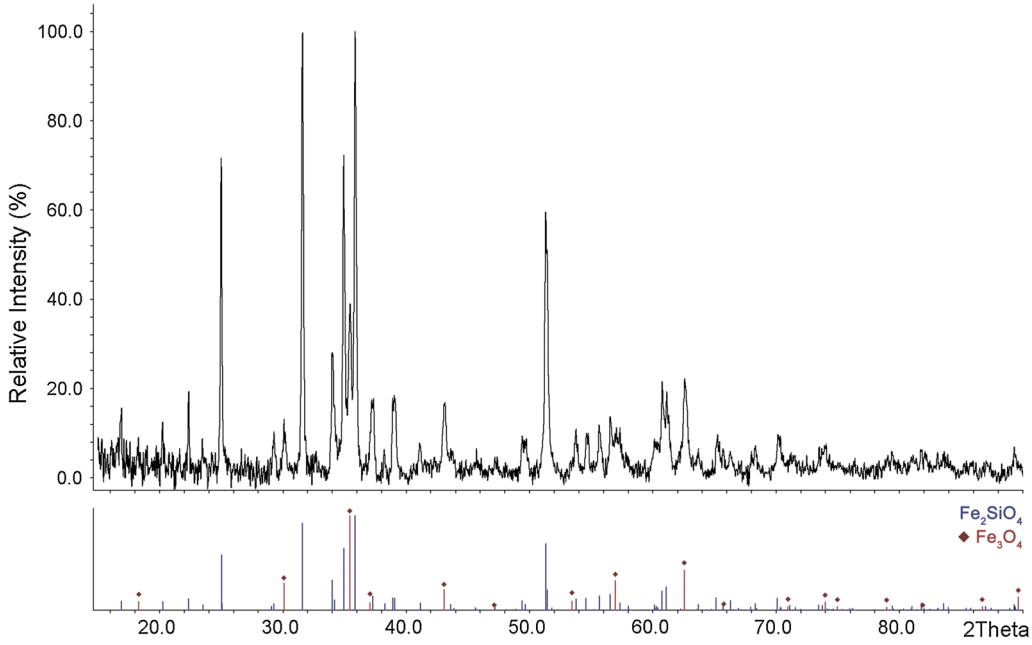

Fig. 10—A typical XRD pattern (sample #5).

Table II. The Phases Found in the Samples ##1–8 by SEM EDS and XRD

	Fe_2SiO_4		Cu-Fe Sulfides		Fe_3O_4		"Glass"	Other Phases	
Sample	SEM	XRD	SEM	XRD	SEM	XRD	SEM	SEM	XRD
#1	x	x	x	x (P)	x	x	x	—	—
#2	x	x	x	x (C)	x	x	x	Pb sulfide	—
#3	x	x	x	x (C)	x	x	x	Pb,Zn sulfides	—
#4	x	x	x	x (RMC)	x	—	x	Pb,Mo sulfides	—
#5	x	x	x	—	x	x	x	Pb,Zn sulfides	$CuFeO_2$
#6	x	x	x	x (MB)	x	—	—	$KAlSi_2O_6$; Pb, Zn sulfides	$CuFe_2O_4$,
#7	—	x	—	—	—	x	x	SiO_2; Zn sulfide	SiO_2
#8	x	x		x (N)	x	x	x	Zn sulfide	—

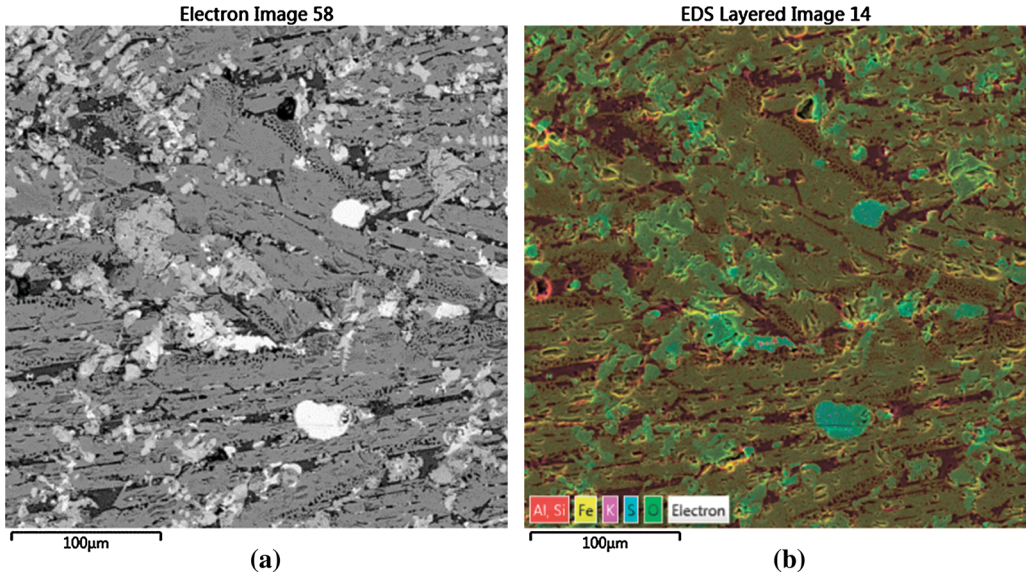

Fig. 11—The SEM image (*a*) and phase composition (*b*) for sample #4.

Table III. The Phase Composition by SEM EDS for Sample #4

Phase	Marked	Percent	O	Al	Si	S	K	Ca	Fe	Cu	Zn
Fayalite	FeOSi	75.2	bal.	1.16	13.87	0.25	0.48	0.49	27.8	0.1	0.2
Glass	FeSiO	12.4	bal.	5.9	16.56	0.86	5.60	2.17	12.6	0.28	0.21
Complex Sulfides	FeSZn	2.4	bal.	—	1.17	38.8	—	—	27.1	4.6	16.15
	FeS	7.5	bal.	1.25	3.84	30.2	0.69	0.43	33	3.46	0.58
	CuFeS	0.1	bal.	0.75	2.69	25.7	0.27	0.33	16.5	30.7	—
Magnetite	FeO	2.1	bal.	2.34	4.75	4.09	0.36	0.49	35.7	1.82	0.41

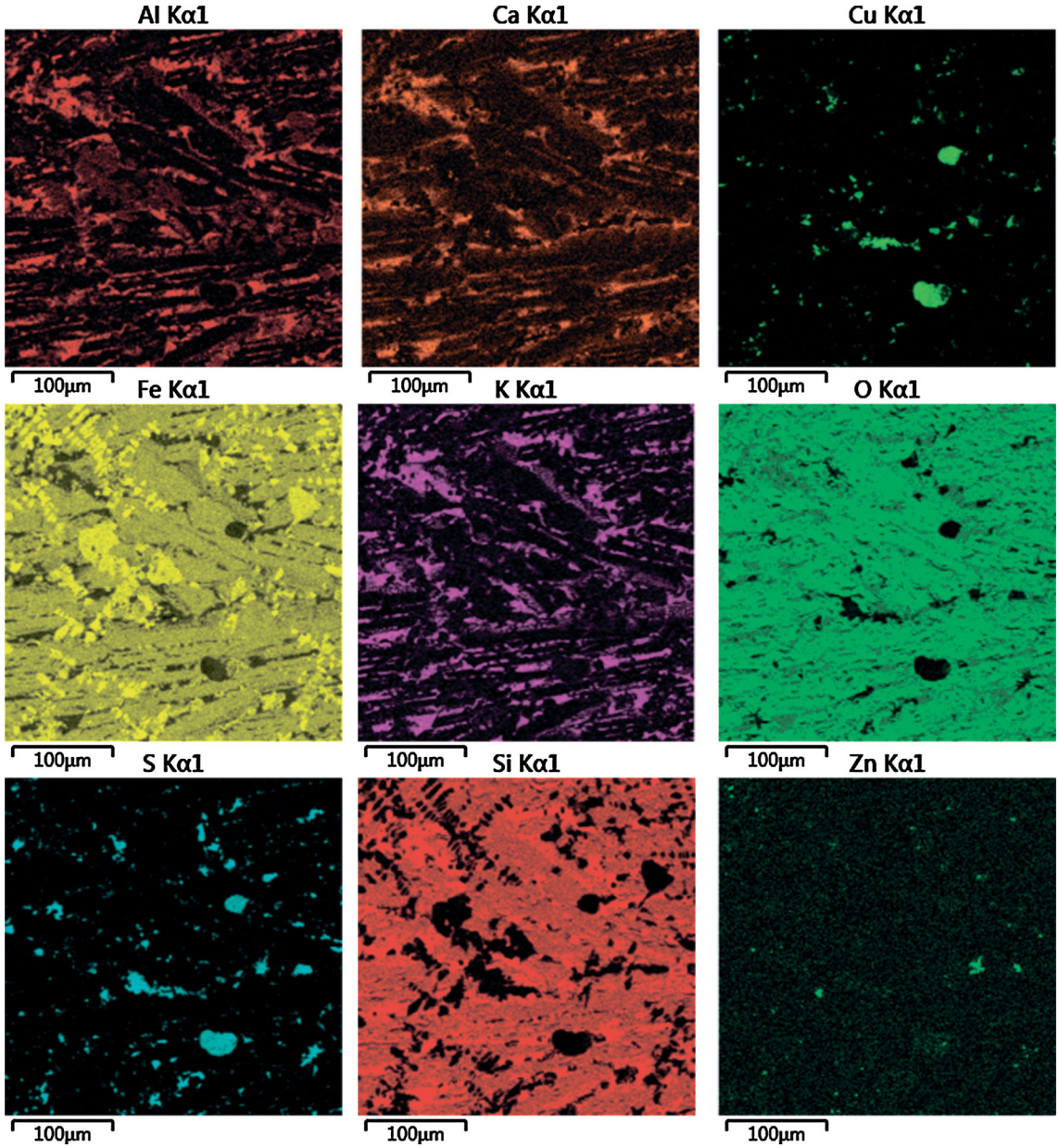

Fig. 12—Element mapping of the same area of sample #4.

The zone D of sample #9 is closest to the ladle steel bottom. Due to a high cooling rate this slag solidifies very rapidly, and the sample has a very disperse microstructure. It can be seen from Figure 22 that the fayalite crystals are indeed very fine (estimated size is 0.6 to 0.8 μm). The amount of copper in the zone D determined by XRF and wet chemistry is 0.93 ($\pm$0.02) and 0.85 ($\pm$0.01) wt pct, respectively.

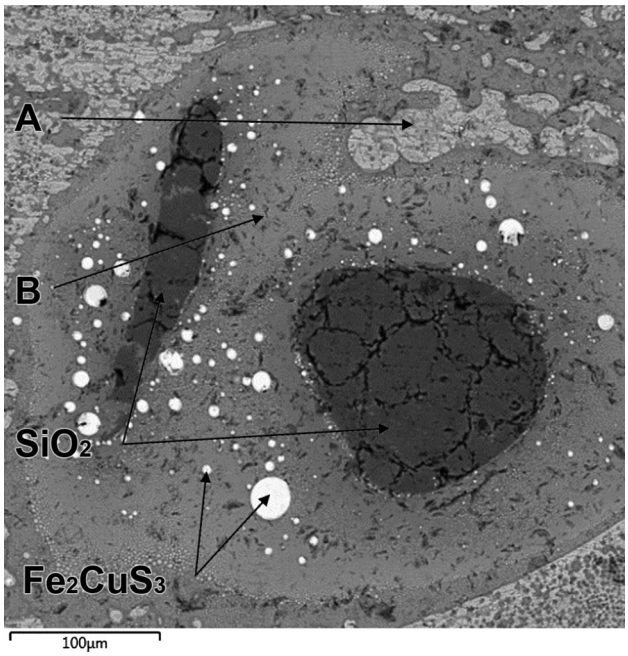

Fig. 13—Example of microstructure for sample #7.

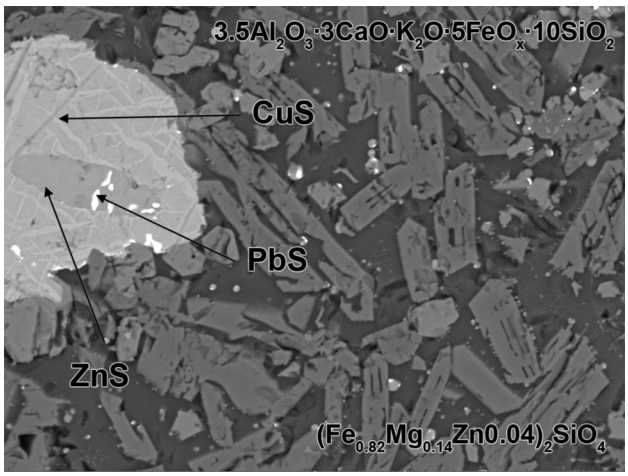

Fig. 14—Example of Pb and Zn sulfides present in the slag sample 3.

Microstructure investigation revealed that the bottom crust is actually formed in several steps. First of all, the zone D is formed as slag starts pouring into the ladle. Because of a high temperature gradient, it is solidified immediately and forms a quenched layer of slag. When the ladle is being filled with the rest of slag, sulfides previously dissolved in the slag precipitate out on cooling. With time sulfide droplets settle down to the ladle bottom, solidify, and formed the zone B, rich in copper and sulfur. While the ladle is being transported to the deposition site, the process of sulfides settling is promoted by gravitation and vibrations of the carriages. As the crust formed the slag adjacent to it may remain liquid. The origin of the solid interface between two zones B is not certain.

E. *Modeling of Copper Smelting Slags*

Microscopic study showed that all the slag samples contain copper sulfide particles of different sizes varying from tens of μm to hundreds μm. These particles precipitate out of the liquid slag during slag crystallization on cooling. Moreover, it is apparent that crystallization of slag samples during the copper smelting process occured in nonequilibrium conditions. Even in the case, modeling of thermodynamic equilibria in slags can still provide interesting information about the process conditions and performance. In addition to that, calculations of the settling rates of sulfide particles based on the predicted slag viscosity can also provide some insights into entrainment of the matte droplets in a liquid slag.

Equilibrium crystallization of the quenched slag sample (#10) calculated by MTDATA in air is shown on Figure 23. It can be seen that at high temperatures the sample consists only of one liquid (slag) phase with dissolved Cu. At lower temperatures Cu transfers into the liquid sulfide phase. A small amount of the other liquid (sulfide) phase appears at ~1773 K (1500 °C) and crystallizes at ~1433 K (1160 °C). The liquidus temperature of the slag phase is around 1573 K (1300 °C); at this temperature the tridymite (SiO_2) phase starts to form. The second phase to crystallize out of the liquid slag is fayalite (Fe_2SiO_4). However, since the actual slag sample was rapidly quenched it is not in equilibrium, and the tridymite phase has not been formed and a glassy phase may have been formed instead. As indicated above fine crystals of the fayalite phase may have still been precipitated out of the slag or glass phase.

As indicated above the liquid sulfide (or matte) phase is stable down to ~1433 K (1160 °C), which implies that Cu sulfide particles were liquid during the rapid solidification. The amount of the Cu sulfide phase is rather small and apparently cannot be detected by XRD.

Other examples of the equilibrium crystallization curves calculated for the slag samples #2 and #4 are shown in Figures 24 and 25, respectively. The sample #4 represents "true fayalite" slag and the sample #2 is richer in the SiO_2 content (see Figure 1). It can be seen that during equilibrium crystallization a first phase that precipitates out for the sample #2 is the SiO_2 phase (tridymite). Fayalite is present in both samples, but sample #4 consists of more than 60 wt pct fayalite at room temperature. Other predicted phases include two spinel-like phases: first with Zn, second with Ti. For both samples the liquid sulfide phase precipitates out of the liquid slag at high temperatures (ca. 1973 K and 2173 K (1700 °C and 1900 °C), respectively). Slag samples collected at the slag deposition site are most likely not to be in equilibrium, as emptying of a slag ladle implies a rapid cooling of the slag.

Generally, the equilibrium calculations for the sample #4 are in good comparison with the phase composition determined by the SEM EDS method (see Table III). The calculated amount of fayalite is over 60 wt pct, which is close to that determined by SEM EDS. The predicted sulfide phase content (digenite, chalcopyrite, and pyrrhotite at low temperatures, and liquid sulfide at

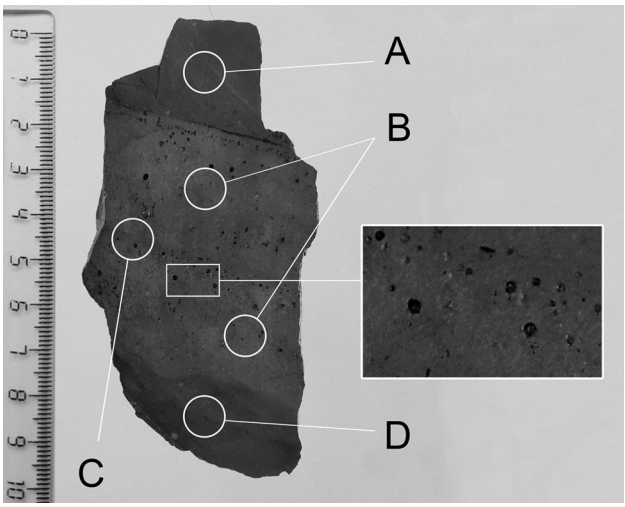

Fig. 15—Cross section of sample #9.

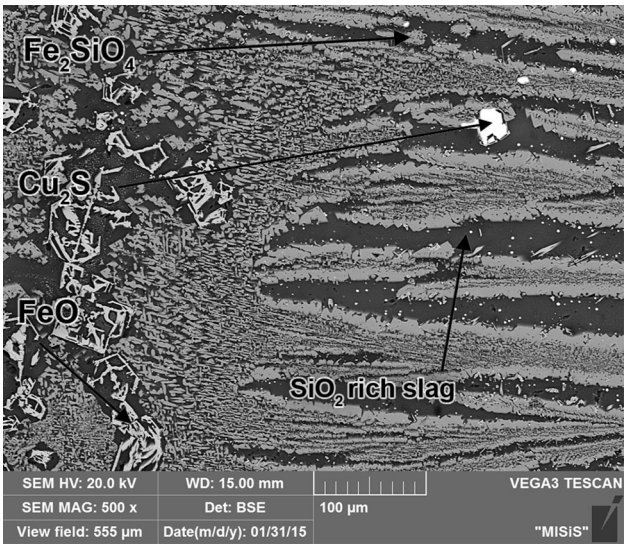

Fig. 16—Microstructure of A-zone.

high temperatures) is also close to the experimentally determined value (Table III).

Viscosity of the liquid slag samples #4, #8, and #10 was calculated by two models: the modified Urbain model[6,7] and Utigard–Warczok model.[8] The slag viscosities as a function of temperature are shown in Figure 26. It was assumed for simplicity that slags are supercooled liquids below the liquidus temperatures. It can be seen from Figure 26 that the sample #10 has a maximum viscosity, because the SiO_2 content in this slag is higher than that in #4 and #8. It can also be seen that two models provide similar results.

The settling rates of matte droplets in the slag liquid were calculated by the Hadamard–Rybczynski formula[4]:

$$V = (\rho_M - \rho_S) g r^2 / 3\eta_S,$$

where ρ_M and ρ_S are the densities of the matte and slag phases, respectively, r is the droplet radius, and η_S

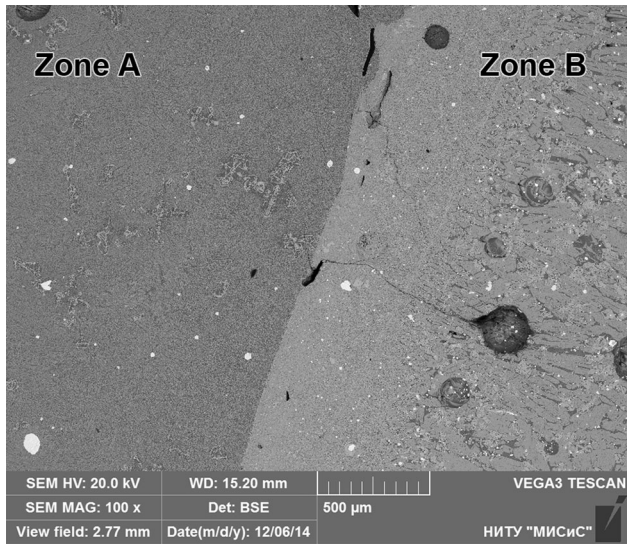

Fig. 17—The A–B interface.

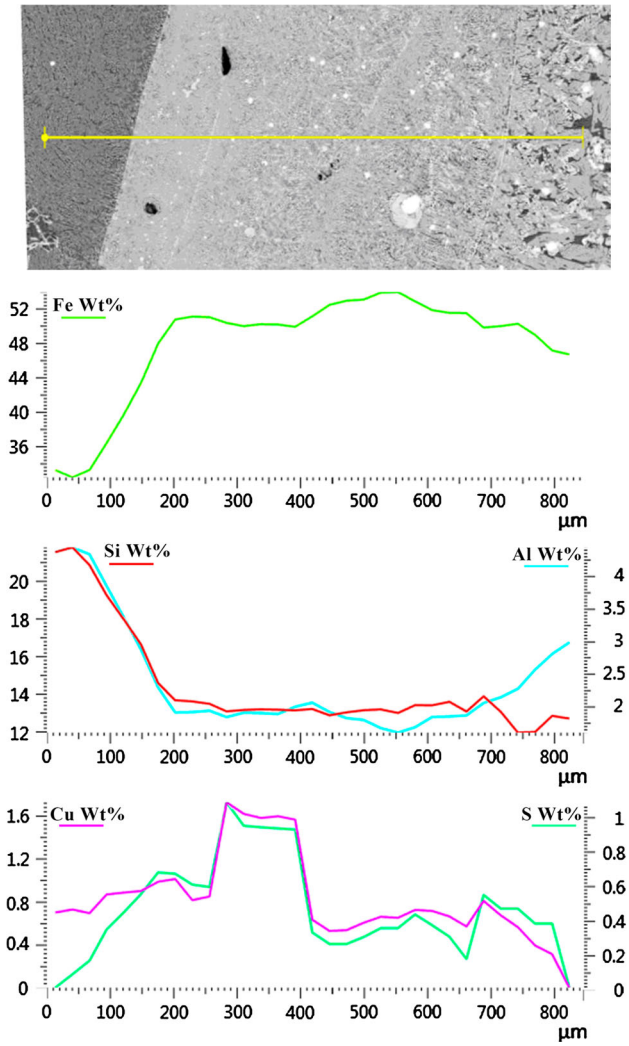

Fig. 18—Element distribution in the A–B interface.

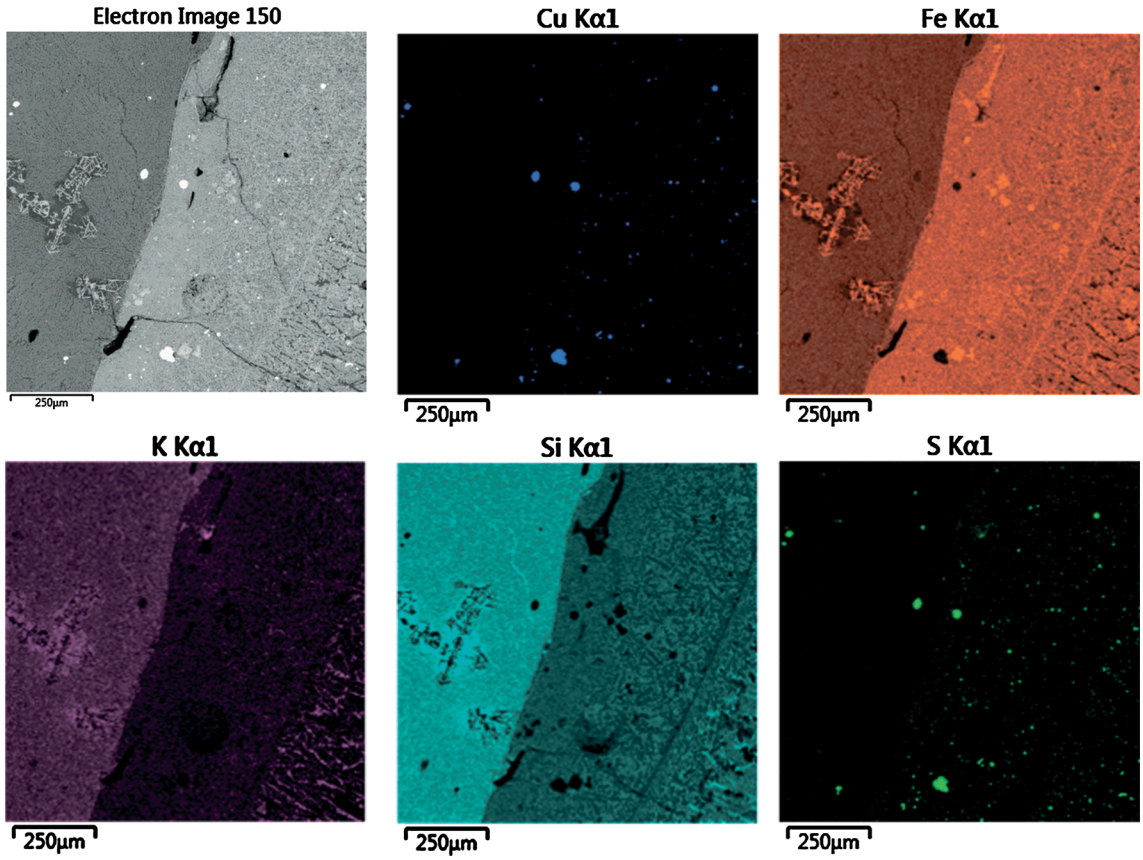

Fig. 19—Elemental mapping of the A and B zones interface.

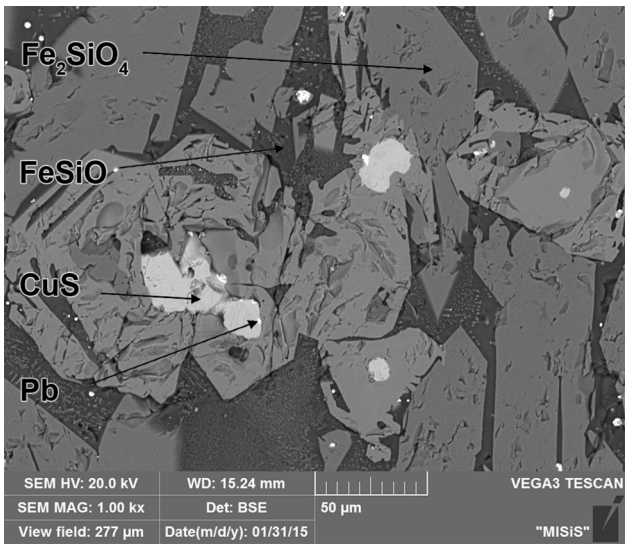

Fig. 20—Microstructure of the zone B.

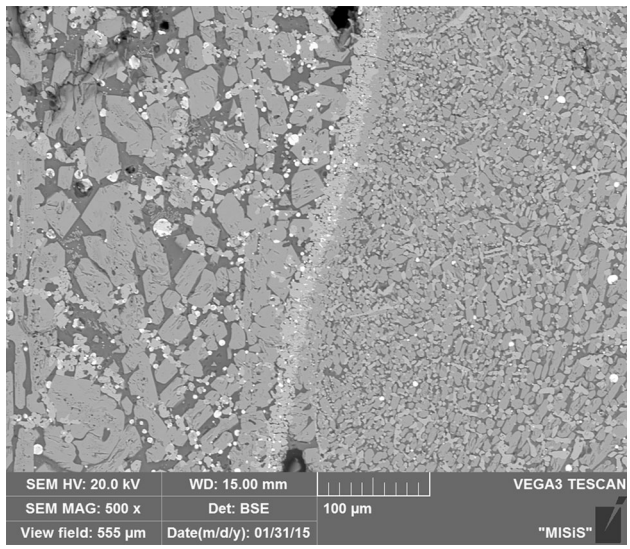

Fig. 21—The microstructure close to the interface C.

is the slag viscosity. The calculation results for the droplet radii of 10 and 20 μm and the density difference of 1 g/cm^3 are presented in Figure 27 for the slags #4, #8, and #10. It can be seen that the settling rate of matte droplets in the slag #4 is about two orders of magnitude higher than that in the slag #10.

F. *Reduction of Copper Losses*

Analysis of the slag samples collected at the Almalyk copper smelter showed that the copper content in slag samples may vary significantly depending on numerous factors. While the slag samples obtained on tapping may contain the amount of copper that is acceptable for

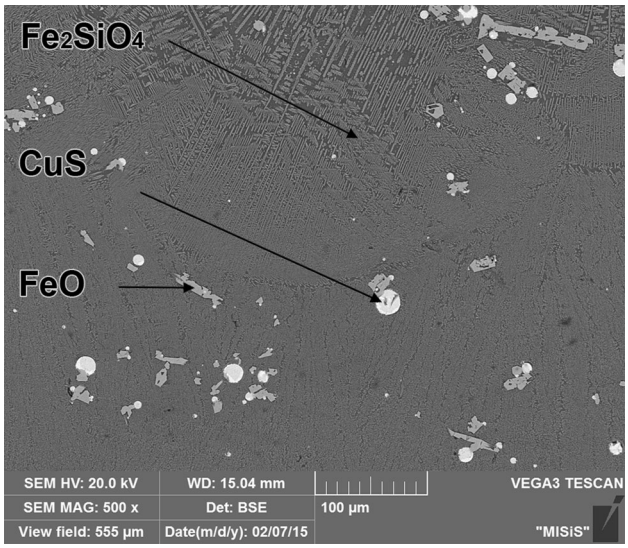

Fig. 22—The microstructure of the zone D.

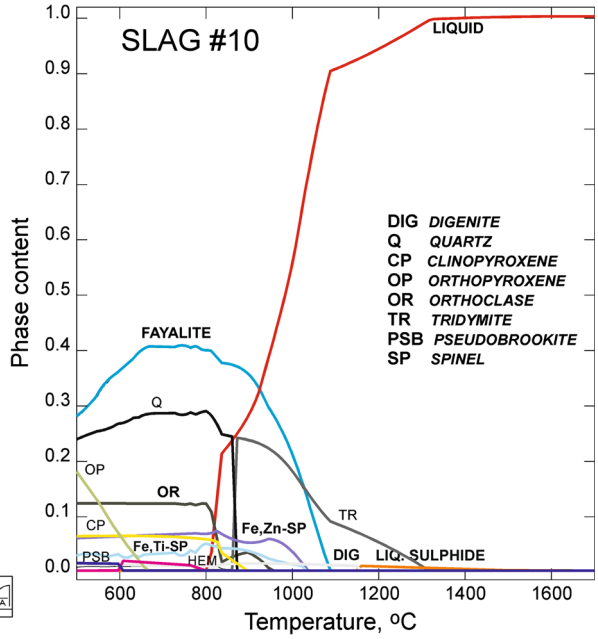

Fig. 23—Equilibrium crystallization of the sample #10.

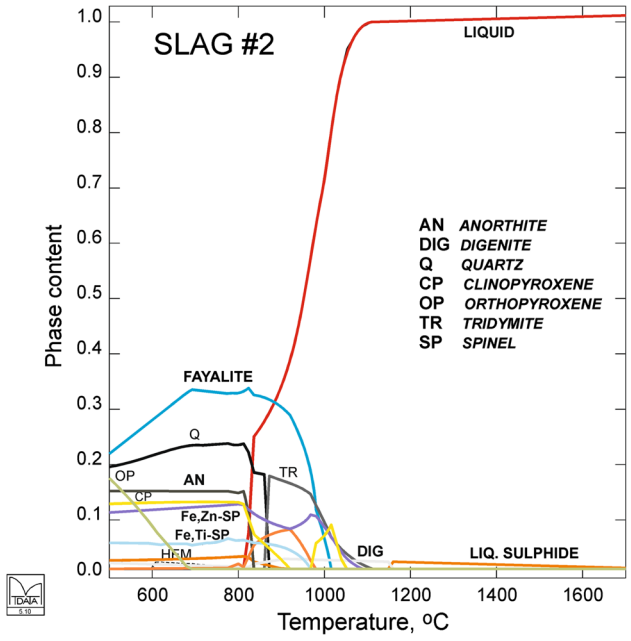

Fig. 24—Equilibrium crystallization of sample #2.

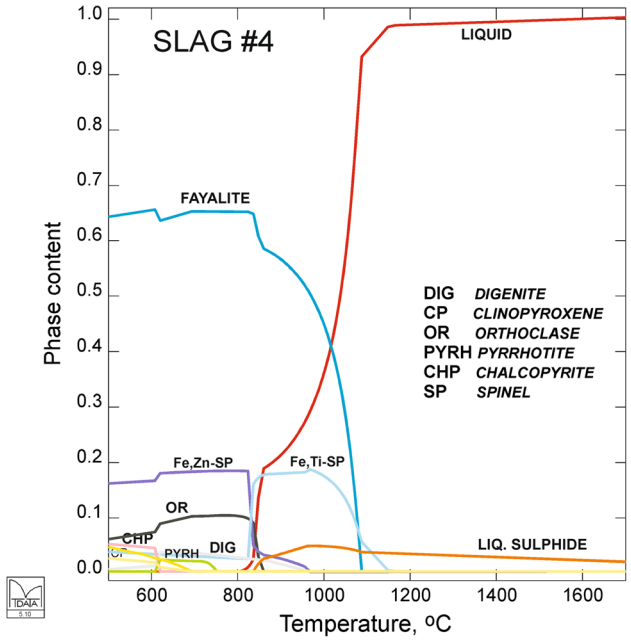

Fig. 25—Equilibrium crystallization of sample #4.

effective smelter operation (*e.g.*, ≤1 wt pct), the slag from the ladle bottom can have very high copper content (2 to 3 wt pct) due to segregation of the sulfide phase from slag.

Apparently the major source of copper losses lays in the formation of the so-called bottom crust during slag tapping and transportation to the deposition site. The bottom crust formed is rich in the sulfide phase (and consequently, copper) and stems from segregation of sulfides from the liquid slag phase. The matte-slag separation is a core of the copper smelting and is governed generally by the thermodynamic driving force, difference in the specific gravity of the slag and sulfide phases, and such properties of the liquid slag like viscosity and surface tension. Since the separation process cannot be avoided, the only ways to reduce copper losses in a slag ladle are either to enhance sulfide segregation inside the furnace or to recycle the slag partially (the bottom crust) or completely.

Analysis of the slag samples also showed that almost all Cu is present in the samples as sulfide particles. No dissolved Cu was found to be in the crystallized oxide phases such as fayalite or magnetite, and the glass-like phase can occasionally contain up to 0.5 to 0.6 wt pct of

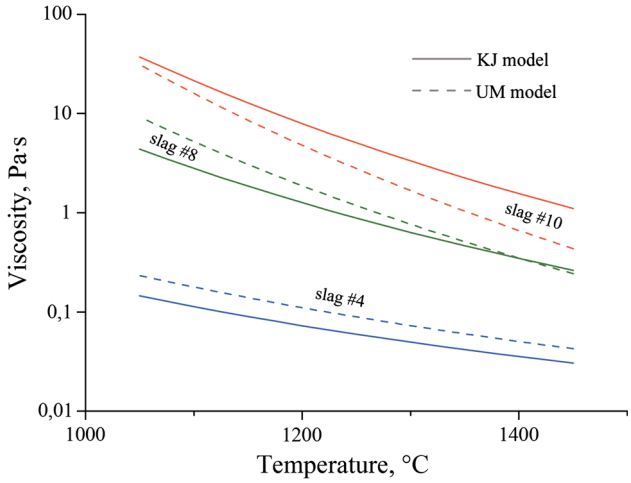

Fig. 26—Viscosity of the liquid slag samples as a function of temperature.

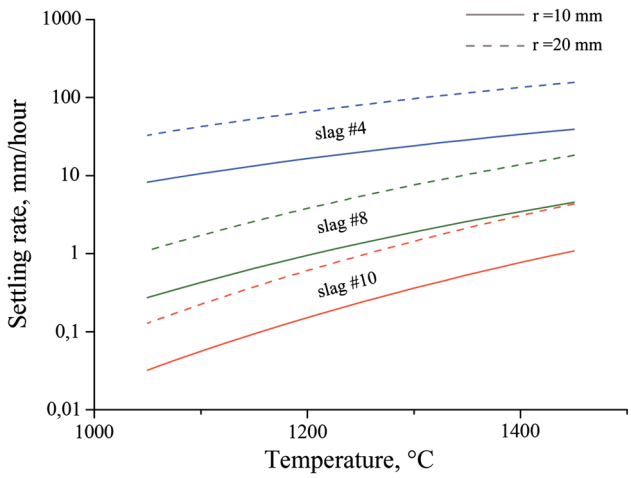

Fig. 27—The settling rates of the matte droplets as a function of temperature.

Cu. Since the proportion of the glass phase in a sample is about 10 to 15 wt pct, this implies that the Cu amount dissolved in the slag phase is rather negligible (less than 0.01 wt pct). Even in the quenched sample (#10) the amount of dissolved Cu was found to vary within 0.3 to 0.8 wt pct, while most of Cu seems to be precipitated as sulfide particles (for example, see Figure 4). Similar finding was reported for slag samples quenched in water.[1]

It is known that most of Cu (approximately 75 pct at 1473 K (1200 °C)) is dissolved in the slag phase at high temperatures.[9] However, it was found that during relatively slow cooling, which is normally the case for industrial slags, most of Cu precipitate out of the slag phase as sulfide particles (droplets). Moreover, the amount of Cu present in the slag at high temperatures as sulfide droplets depends on the slag chemical composition.

There are not many parameters of the process that can be tuned up to enhance the matte-slag separation in the smelter. It can be seen from thermodynamic calculations that the onset temperature of precipitation of the liquid sulfide phase can vary significantly depending on the slag composition. Specific gravity decreases with increasing Fe content in the sulfide phase, which in turn reduces the matte grade and therefore is not desirable. Estimation of the slag viscosity and the settling rates of matte droplets demonstrate that the slag/matte separation in slags with lower SiO_2 content is significantly faster than in slags with higher SiO_2. Viscosity and surface tension of the liquid slag (and as a result the settling rate of matte drops) can also be lowered using additives like CaO or MgO.

IV. CONCLUSIONS

In the present paper the microstructure and phase composition of slags from the Almalyk copper flash smelter were investigated experimentally by different methods (LOM, XRD, SEM, and XRF) and then modeled to obtain detailed understanding of the copper smelting process and to evaluate potential ways of its improvement. The slag samples were taken at different stages of the Almalyk copper smelting process.

It was found that the copper content in the slags may vary significantly depending on the location of slag sampling. Cu was found to be present as sulfide particles, almost no Cu is dissolved in the slag. Analysis of microstructure and phase composition by SEM EDS showed that major phase found in the samples is fayalite, while other phases are complex spinels (including magnetite), different sulfides, and an amorphous phase. Thermodynamic calculations demonstrated the presence of these phases, their compositions, and optimal ranges of operating conditions. Analysis of the slag samples revealed that some of them are fayalite slags, but the others may differ significantly from the fayalite composition.

Examination of the samples from the ladle bottom showed the presence of segregation in the chemical composition of the sample. Area with the highest amount of copper in it is close to the bottom of the ladle. It was concluded that the segregation in the chemical composition is the reason for discrepancy in amounts of copper in samples taken from the tapping and on the slag disposition.

It was found that Pb is present only in the sulfide phase, while Zn was observed both in the slag and sulfide phases. Behavior of other minor elements was also analyzed and discussed.

Potential ways of reducing copper losses and optimizing the smelting process were suggested on the basis of the overall investigation.

ACKNOWLEDGMENTS

The work was carried out with financial support from JSC Almalyk GMK and from the Ministry of Education and Science of the Russian Federation in the

framework of Increase Competitiveness Program of NUST MISIS (No. K2-2014-014) and of the basic part of the state program Organisation of the Research Work for higher educational institutions in 2014–2016.

REFERENCES

1. H. Jalkanen, J. Vehvilainen, and J. Poijarvi: *Scand. J. Metall.*, 2003, vol. 32, pp. 65–70.
2. R.H. Davies, A.T. Dinsdale, J.A. Gisby, J.A.J. Robinson, and S.M. Martin: *CALPHAD*, 2002, vol. 26, pp. 229–71.
3. The International Centre for Diffraction Data: *PDF-2 Database, Release 2014*. http://www.icdd.com/products/pdf2.htm, 2014. Accessed 16 Nov 2015.
4. M.E. Schlesinger, M.J. King, K.C. Sole, and W.G. Davenport: *Extractive Metallurgy of Copper*, 5th ed., Elsevier, ISBN 978-0-08-096789-9, 2011, pp. 1–455.
5. S. Vaisburd, A. Berner, D.G. Brandon, S. Kozhakhmetov, E. Kenzhaliyev, and R. Zhalelev: *Metall. Mater. Trans. B*, 2003, vol. 33B, pp. 551–59.
6. A. Kondratiev and E. Jak: *Metall. Mater. Trans. B*, 2001, vol. 32B, pp. 1015–25.
7. L. Forsbacka, L. Holappa, A. Kondratiev, and E. Jak: Steel Res*Int*., 2007, vol. 78 (9), pp. 676–84.
8. T.A. Utigard and A. Warczok: *Proceedings of COPPER 95—COBRE 95 International Conference*, vol. 4, W.J. Chen, C. Diaz, A. Luraschi, and P.J.Mackey, eds., Metallurgical Society of CIM, 1995, pp. 423–37.
9. P. Coursol, N.C. Valencia, P. Mackey, S. Bell, and B. Davis: *JOM*, 2012, DOI:10.1007/s11837-012-0454-6.